Title
Initial B Cell Activation Induces Metabolic Reprogramming and Mitochondrial Remodeling

Authors
Waters, Lynnea R
Ahsan, Fasih M
Wolf, Dane M
et al.

Publication Date
2018-07-01

DOI
10.1016/j.isci.2018.07.005

Peer reviewed

iScience

CellPress

Article

Initial B Cell Activation Induces Metabolic Reprogramming and Mitochondrial Remodeling

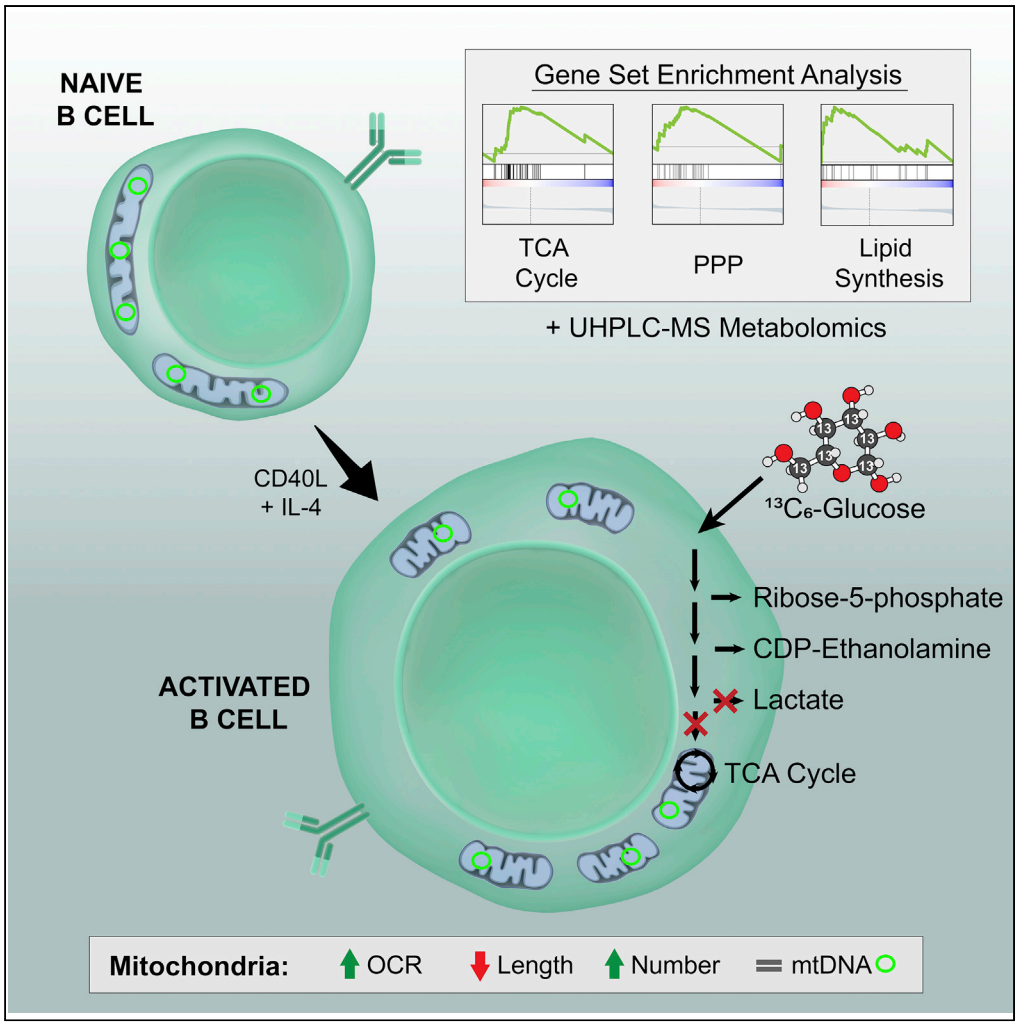

Lynnea R. Waters, Fasih M. Ahsan, Dane M. Wolf, Orian Shirihai, Michael A. Teitell

mteitell@mednet.ucla.edu

HIGHLIGHTS

Glucose is dispensable for B cell activation; OXPHOS is fueled by other nutrients

Few, elongated mitochondria remodel to many punctate mitochondria upon activation

mtDNA and nucleoid numbers remain similar for naive and 24 hr stimulated B cells

Combined RNA-seq and metabolomics used to study metabolism during B cell activation

Waters et al., iScience 5, 99–109
July 27, 2018
https://doi.org/10.1016/j.isci.2018.07.005

iScience

CellPress

Article

Initial B Cell Activation Induces Metabolic Reprogramming and Mitochondrial Remodeling

Lynnea R. Waters,[1,2] Fasih M. Ahsan,[2] Dane M. Wolf,[3,4,5] Orian Shirihai,[3,4,5] and Michael A. Teitell[1,2,6,7,*]

SUMMARY

B lymphocytes provide adaptive immunity by generating antigen-specific antibodies and supporting the activation of T cells. Little is known about how global metabolism supports naive B cell activation to enable an effective immune response. By coupling RNA sequencing (RNA-seq) data with glucose isotopomer tracing, we show that stimulated B cells increase programs for oxidative phosphorylation (OXPHOS), the tricarboxylic acid (TCA) cycle, and nucleotide biosynthesis, but not glycolysis. Isotopomer tracing uncovered increases in TCA cycle intermediates with almost no contribution from glucose. Instead, glucose mainly supported the biosynthesis of ribonucleotides. Glucose restriction did not affect B cell functions, yet the inhibition of OXPHOS or glutamine restriction markedly impaired B cell growth and differentiation. Increased OXPHOS prompted studies of mitochondrial dynamics, which revealed extensive mitochondria remodeling during activation. Our results show how B cell metabolism adapts with stimulation and reveals unexpected details for carbon utilization and mitochondrial dynamics at the start of a humoral immune response.

INTRODUCTION

B and T lymphocytes are key effector cells in an adaptive immune response. Both cell types express unique surface receptors that recognize an immense repertoire of antigens. Upon antigen recognition, B cells upregulate surface molecules that support the activation of T cells, including those for antigen presentation through major histocompatibility complex class II (MHC class II) and those for co-stimulation by CD86/B7-2. T cell-dependent B cell activation leads to selective recruitment into transient anatomical sites of differentiation known as germinal centers (GCs). In GCs, B cells proliferate and edit their antigen receptors to refine and augment a humoral immune response. This gene editing includes somatic hypermutation, which increases antibody specificity, and isotype class switch recombination (CSR), which exchanges the immunoglobulin heavy chain constant region to support specific antibody functions. Ultimately, GC B cells differentiate into long-lived plasma cells that secrete antibodies or into memory B cells that re-activate with antigen re-engagement, providing a basis for vaccination.

The metabolic requirements for initially activated B cell proliferation and differentiation are relatively unknown (reviewed in Table S1). Naive B cells are maintained in a quiescent state, and activation initializes cellular reprogramming to drive re-entry into the cell cycle. Rapid cell expansion requires production of biomolecules including proteins, lipids, and nucleotides at an extraordinary rate. The details for how activated B cells support a rapidly increasing biomass are unknown. Two recent reviews expressed a critical need for studies of metabolic pathways supporting B cell activation (Boothby and Rickert, 2017; Jellusova and Rickert, 2017). Stimulation of B cells with lipopolysaccharide (LPS), a Toll-like receptor (TLR) 4 receptor agonist, or an anti-IgM antibody, to cross-link the B cell antigen receptor, increases glucose import into activated B cells and leads to an increased oxygen consumption rate (OCR) (Caro-Maldonado et al., 2014; Cho et al., 2011; Doughty et al., 2006; Dufort et al., 2007; Jellusova et al., 2017). How imported glucose is utilized, and whether T cell-dependent B cell activation utilizes similar pathways remain unknown. More than a decade ago, Doughty and colleagues utilized isotopomer-labeled glucose in IgM-stimulated B cells to show that glucose shuttled into the pentose phosphate pathway (PPP), but reported results for only two metabolites, lactate and glutamate (Doughty et al., 2006). To date there are no studies that globally examine metabolism or glucose fate upon initial B cell activation beyond these individual measures.

Despite reports of increased oxygen consumption in multiple B cell stimulation conditions, little is known about how quiescent B cells alter their mitochondria to support increased oxidative phosphorylation

[1]Molecular Biology Interdepartmental Program, University of California, Los Angeles, Los Angeles, CA 90095, USA

[2]Department of Pathology and Laboratory Medicine, University of California, Los Angeles, Los Angeles, CA 90095, USA

[3]Department of Molecular and Medical Pharmacology, University of California, Los Angeles, Los Angeles, CA 90095, USA

[4]Division of Endocrinology, Department of Medicine, David Geffen School of Medicine, University of California, Los Angeles, Los Angeles, CA 90095, USA

[5]Department of Medicine, Boston University School of Medicine, Boston, MA 02118, USA

[6]Department of Pediatrics, Department of Bioengineering, Broad Stem Cell Research Center, Jonsson Comprehensive Cancer Center, and California NanoSystems Institute, University of California, Los Angeles, Los Angeles, CA 90095, USA

[7]Lead Contact

*Correspondence: mteitell@mednet.ucla.edu

https://doi.org/10.1016/j.isci.2018.07.005

(OXPHOS). Both T cell-dependent and T cell-independent stimulation have been observed to increase staining with membrane potential-dependent dyes, by immunofluorescence or flow cytometry. However, the resolution achieved fails to discriminate between fluorescence increases due to increases in mitochondrial mass versus an increase in membrane potential, or both. Recent studies in T lymphocytes have demonstrated major remodeling upon activation (Ron-Harel et al., 2016), although it remains unclear whether mitochondrial remodeling also occurs with or without similar dynamics for B lymphocytes to support a shift from quiescence to activation. Therefore, we examined primary mouse B cell metabolism using a well-established *in vitro* model of B cell activation that replicates a B cell interaction with T cells through co-stimulation of surface CD40 and addition of the T cell cytokine, interleukin (IL)-4 (Rush and Hodgkin, 2001). By combining publicly available RNA sequencing (RNA-seq) data with mass spectrometry (MS) tracing of glucose and intracellular metabolites, we report on key metabolic networks and requirements for B cell metabolism during early B cell activation.

RESULTS

Activated B Cells Increase Glucose Uptake but Do Not Accumulate Glycolytic Metabolites

To isolate B cells, we sorted $CD43^-$ cells from total mouse splenocytes (Figure S1A), resulting in a 97% pure $CD19^+$ $B220^+$ $CD4^-CD8^-$ naive B cell population (Figure S1B). After 24 hr of stimulation with CD40L and IL-4 (Rush and Hodgkin, 2001), flow cytometry analysis confirmed that B cells had undergone an increase in cell size as measured by forward scatter (FSC-A) and induction of activation markers including MHC class II, required for antigen presentation to T cells, and CD86/B7-2, a costimulatory molecule required for T cell activation (Figure S1C).

Previous studies have shown that B cells increase glucose import with activation (Caro-Maldonado et al., 2014; Cho et al., 2011; Doughty et al., 2006; Dufort et al., 2007). In agreement, we also measure an increase in import of the fluorescent glucose analog, 2-Deoxy-2-[(7-nitro-2,1,3-benzoxadiazol-4-yl)amino]-D-glucose (2-NBDG), in CD40/IL4 activated B cells (Figure 1A). To investigate carbon utilization from glucose, we performed metabolite tracing in naive and stimulated B cells. Growing cells in media with $^{13}C_6$-glucose enables tracing of carbons by analyzing the shifts in mass peaks of metabolites through MS (Table S2). We observe that 90% of glucose was fully m+6 labeled in both conditions, confirming import of the glucose label (Figure 1B). Multiple published reports suggest or assume that glycolysis is upregulated upon B cell activation (Caro-Maldonado et al., 2014; Doughty et al., 2006; Garcia-Manteiga et al., 2011; Jellusova et al., 2017). Unexpectedly, however, the total levels of glycolytic metabolites decrease upon activation, with the exception of 3-phosphoglycerate (3PG) (Figure 1C). Of note, lactate levels do not increase at 24 hr as expected with upregulation of glycolysis. We also investigated the isotopologue distribution in glycolytic metabolites. Despite decreases in the total amounts of glycolytic metabolites, we measured increased m+6 label in glucose-6-phosphate/fructose-6-phosphate and fructose-1,6-bisphosphate, and increased m+3 label in G3P and 3PG for activated versus naive B cells (Figure 1D). These results suggest that glucose is fluxing through the glycolytic pathway, although not accumulating, and is likely routed into alternative metabolic pathways in activated B cells.

Since multiple studies have found that glucose uptake is increased upon B cell activation (Caro-Maldonado et al., 2014; Cho et al., 2011; Doughty et al., 2006; Dufort et al., 2007), we sought to determine the functional outcome of glucose limitation by culturing B cells in media lacking glucose. For these studies low-level, >10-fold reduced, residual glucose (1.5 mM, data not shown) was unavoidably present from the media fetal bovine serum (FBS). Surprisingly, there was a small to absent impact of limiting glucose on B cell activation, differentiation, or proliferation (Figure 1E). B cells cultured in residual FBS glucose showed a defect in class switching to IgG1; however, glucose appeared dispensable in culture for other B cell functions (Figure 1E).

OXPHOS and TCA Cycle Elevation

Prior studies of metabolism during B cell activation provide an incomplete evaluation of metabolic reprogramming in B cells. To determine which metabolic pathways are upregulated, and thus likely active, we performed gene set enrichment analysis (GSEA) on a previously published RNA-seq dataset containing naive and 24 hr activated B cells stimulated by CD40L and IL-4 (GEO: GSE77744) (Wöhner et al., 2016). We identified 56 metabolic Kyoto Encyclopedia of Genes and Genomes (KEGG) pathways comprising between 15 and 500 genes each, and 12 enriched metabolic pathways with a false discovery rate < 0.25 (Tables 1 and S3). Aminoacyl tRNA synthesis (KEGG: MMU00970) was the most enriched pathway and includes transcripts for all tRNA synthetase subunits. This result is concordant with a general increase in protein translation during the transition from a quiescent to a rapidly dividing cell (Vander Heiden et al., 2011).

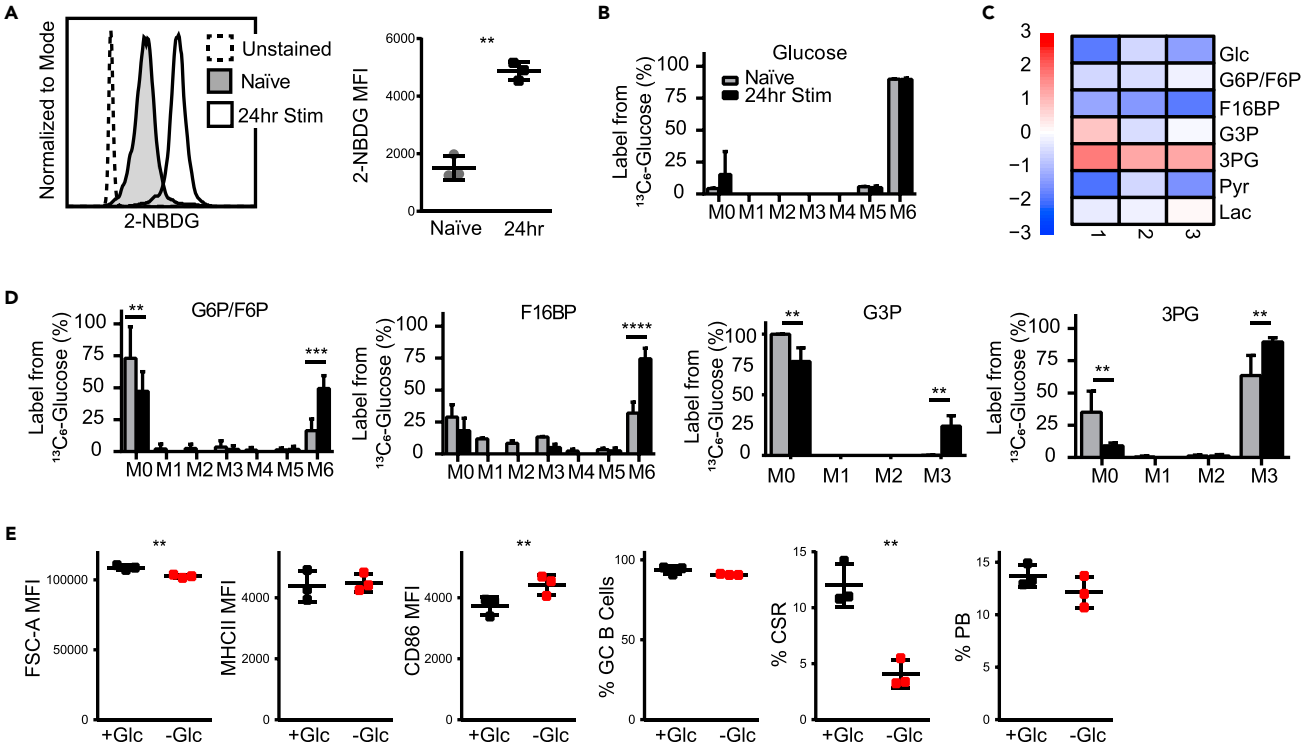

Figure 1. B Cell Activation Induces Glucose Import without Accumulation of Glycolytic Metabolites; Glucose Restriction Has Only Minor Impacts on B Cell Function

(A) Representative flow cytometry plot and quantification of 2-NBDG glucose import into naive and stimulated B cells with unstained control (n = 3).

(B) Isotopomer distribution for labeled glucose in naive and stimulated B cells (n = 3).

(C) UHPLC-MS quantification of relative levels of glycolytic metabolites between stimulated and naive B cells, data shown are $\log_2$ converted average values of 3 technical replicates of 3 biological replicates (n = 3).

(D) Isotopomer distribution for labeled glucose in glycolytic metabolites in naive and stimulated B cells (n = 3).

(E) Flow cytometry analysis of cell size (FSC-A), activation markers (MHCII, CD86) at 24 hr, germinal center differentiation (GC, %B220+ Fas+ GL7+), and class switch recombination (CSR, %B220+ IgG1+) at day 3, and plasmablast differentiation (PB, %B220^{lo} CD138+) at day 5 in cells stimulated with or without glucose (n = 3). Data represent mean ± SD. p Values were determined by a paired two-tailed Student's t test. **p ≤ 0.01; ***p ≤ 0.001; ****p ≤ 0.0001. G6P, glucose-6-phosphate; F6P, fructose-6-phosphate; F16BP, fructose-1,6-bisphosphate; G3P, glycerol-3-phosphate; 3PG, 3-phosphoglycerate; Pyr, pyruvate; Lac, lactate.

Two additional top KEGG pathways were OXPHOS (KEGG: MMU00190) and the tricarboxylic acid (TCA) cycle (KEGG: MMU00020), signifying key roles during B cell activation (Figure 2A). This finding is consistent with prior reports of increased oxygen consumption with B cell activation by LPS or IgM (Caro-Maldonado et al., 2014). To determine whether OXPHOS was also increased with CD40/IL-4 modeled T cell-induced activation, we analyzed the OCR of unstimulated and stimulated B cells. Basal OCR was higher in stimulated B cells than in naive cells, as was maximal respiratory capacity (Figures 2B and S2A). Interestingly, basal OCR of stimulated B cells was almost identical to the maximal OCR of unstimulated B cells (0.717 and 0.684 fmoles O_2/min/cell, respectively). Both subsets of B cells had significant spare respiratory capacity (SRC), which sharply contrasts with activated T cells and naive pre- and pro-B cells that exhibit minimal SRC (Stein et al., 2017; van der Windt et al., 2012). Our data suggest distinct mechanisms of metabolic adaptation for T, immature B, and mature activated B cells.

To further interrogate our transcriptome data mining results that the TCA cycle was upregulated, we measured TCA metabolite levels in stimulated versus naive B cells. We observed an increase in fumarate, malate, and α-ketoglutarate, with little to no change in pyruvate, citrate, or succinate (Figure 2C). We next quantified the isotopomer distribution of TCA cycle metabolites resulting from co-incubation with $^{13}C_6$-glucose. Fully labeled m+3 pyruvate comprised 96% and 97% of the total pyruvate pool in both naive and stimulated B cells, respectively. Inclusion of $^{13}C_6$-glucose and $^{13}C_3$-pyruvate into the TCA cycle would result in accumulations of m+2 peaks for all TCA cycle metabolites (Figure S2B). Surprisingly, examination

KEGG Pathway	ES	NES	Pval	FDR
Aminoacyl tRNA synthesis	0.556	2.215	<0.001	<0.001
Oxidative phosphorylation	0.447	2.183	<0.001	0.002
Terpenoid backbone synthesis	0.645	2.127	<0.001	0.003
Citrate cycle	0.542	2.012	<0.001	0.005
Pentose phosphate pathway	0.486	1.710	0.008	0.049
Biosynthesis of unsaturated fatty acids	0.500	1.728	0.004	0.054
Pyrimidine metabolism	0.333	1.552	<0.001	0.107
One carbon pool by folate	0.453	1.434	0.073	0.190
Cysteine and methionine metabolism	0.372	1.372	0.113	0.236
Glutathione metabolism	0.338	1.331	0.100	0.238
Glyoxylate and dicarboxylate metabolism	0.378	1.286	0.139	0.247
Purine metabolism	0.260	1.301	<0.001	0.249

Table 1. Gene Set Enrichment Analysis (GSEA) for Induced Metabolic Transcripts during B Cell Activation

KEGG metabolism gene set enrichment analysis (GSEA) based on genes differentially expressed between naïve (n = 2) and 24 hr stimulated (n = 2) B cells (GEO: GSE77744). Gene sets were derived from the KEGG database (n = 84, 56 after filtering). Elevated set signatures below a q value of 0.25 are listed (ES, enrichment score; NES, normalized enrichment score; Pval, nominal p value; FDR, FDR adjusted q value).

of five TCA cycle intermediates showed minimal or no labeling in both naive and stimulated conditions (Figure 2D). For example, although there is an increase in the total fumarate level with B cell activation, indicating augmented synthesis of fumarate at 24 hr, only 9% was m+2 labeled in stimulated B cells. This result is despite an increase in the expression of the mitochondrial pyruvate carrier genes, *Mpc1/2* (Figure S2C), which encode for proteins that import pyruvate into mitochondria to supply the TCA cycle, suggesting (not surprisingly) a post-transcriptional regulatory mechanism for pyruvate entry into naive and activated B cells. Increases in OCR and total TCA metabolite levels (Figures 2B and 2C) indicate increased TCA flux; however, labeled glucose and pyruvate are not contributing carbon atoms to these intermediates. Instead, it is likely that activated B cells utilize alternative nutrients to fuel the TCA cycle, which could include lipids, ketones, lactate, or glutamine. Indeed, measurement of glutamine in the culture media shows that B cells import glutamine at a rate of 12.4 μM glutamine/hour/10^6 cells (Figure S2D).

We stimulated naive B cells in the presence of ATP synthase inhibitor, Oligomycin A, to determine the importance of OXPHOS upregulation in activated B cells that are actively increasing biomass. Oligomycin A inhibited B cell size increase and prevented upregulation of B cell activation markers (Figure 3A), suggesting that early activated B cells have coupled mitochondria, and a central role for the TCA cycle and OXPHOS in these processes. At day 3 of modeled T cell stimulation, 10 nM Oligomycin A also completely blocked naive B cell differentiation into GC B cells and immunoglobulin class switching to IgG1. By day 5, cells treated with Oligomycin A were unable to differentiate into plasmablasts (Figure 3A), further supporting the essential role of OXPHOS in B cell activation and differentiation. Since glutamine is robustly imported into activated B cells (Figure S2D) and could fuel the TCA cycle, we investigated the requirement for glutamine during B cell activation by culturing B cells in glutamine-free media. Loss of glutamine causes reductions in activated B cell size, differentiation, class switching, and proliferation (Figure 3B). This result is consistent with findings from Heyse et al. (2015) that show the importance of glutamine for biomass accumulation and DNA replication but not early activation, and is similar to our findings upon inhibition of OXPHOS with Oligomycin A. This, in conjunction with our findings that OXPHOS is increased but not fueled by glucose, suggests that glutamine import fuels the TCA cycle, and is required for B cell activation.

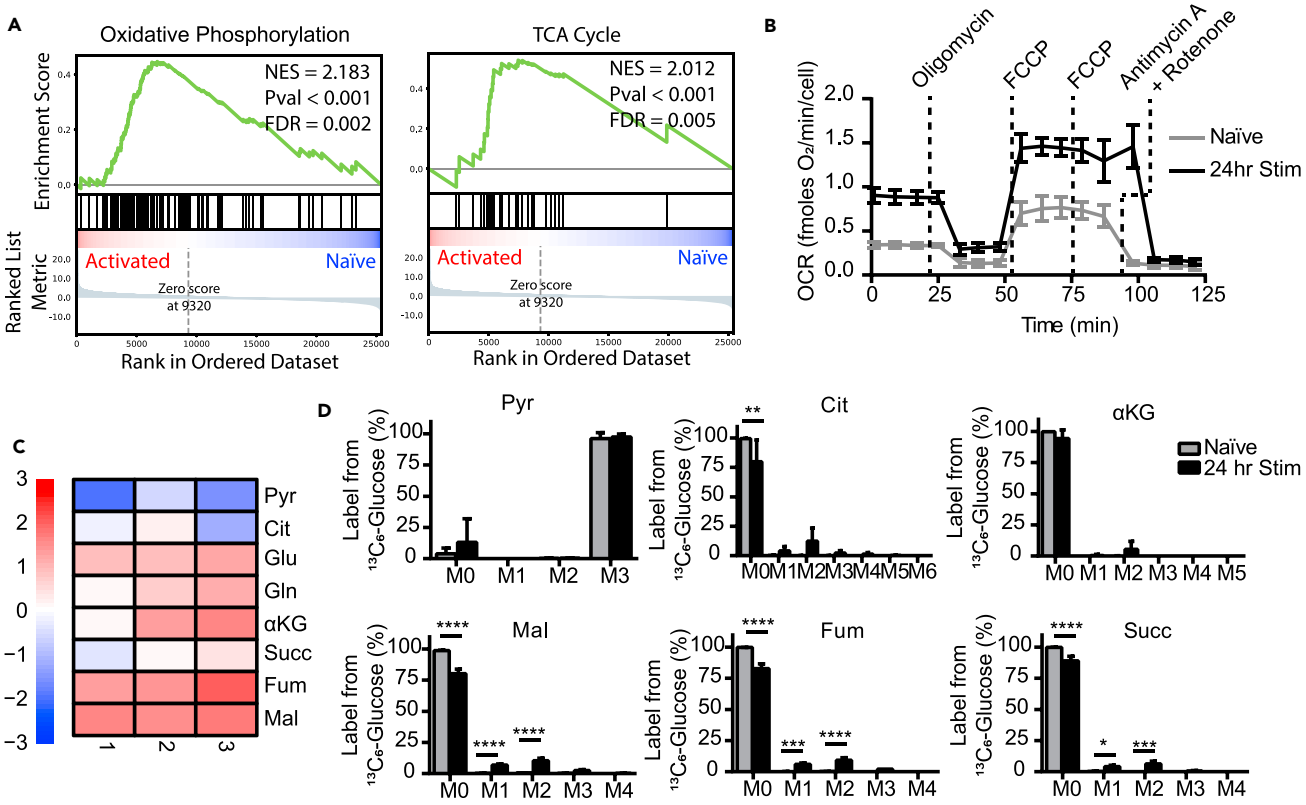

Figure 2. B Cell Activation Induces Increases in OXPHOS and the TCA Cycle

(A) GSEA on RNA-seq transcriptome data from naive and 24 hr stimulated B cells shows enrichment for OXPHOS and TCA cycle metabolic transcripts.

(B) Seahorse extracellular flux analysis measurement of oxygen consumption rate (OCR) in naive and stimulated B cells (n = 4).

(C) UHPLC-MS quantification of $\log_2$ converted average levels of TCA cycle metabolites between stimulated and naive B cells (n = 3).

(D) Isotopomer distribution of labeled glucose for TCA cycle metabolites in naive and stimulated B cells (n = 3). Data represent mean ± SD. p values determined by two-way ANOVA with Bonferroni correction for multiple comparisons. *p ≤ 0.05; **p ≤ 0.01; ***p ≤ 0.001; ****p ≤ 0.0001. Pyr, pyruvate; Cit, citrate; Glu, glutamate; Gln, glutamine; αKG, α-ketoglutarate; Succ, succinate; Fum, fumarate; Mal, malate.

See also Figure S2, Tables S2 and S3.

Glucose Fate(s)

Glucose import increases with naive B cell activation but does not appreciably supply the TCA cycle nor coincides with enrichment of glycolytic genes as measured by GSEA (KEGG: MMU00010) (Figure S3A). Therefore, we analyzed the distribution of glucose carbons through additional metabolic pathways (Figure 4A). Pyruvate is converted to lactate as an end product of glycolysis. However, whereas 97% of pyruvate is m+3 labeled in both naive and activated B cells (Figure 2D), only 31% of total lactate is m+3 labeled (Figure 4B). Interestingly, this is despite increased expression of the lactate to pyruvate conversion enzyme *Ldha* (Figure S3B). Although 31% m+3 label does represent an increase in labeling from naive B cells, it does not fully explain the final fates of carbon during B cell activation. Pyruvate and additional glycolytic intermediates are likely increasing their flux through alternative metabolic pathways. One metabolic pathway that branches from glycolysis is the PPP, which generates ribose-5-phosphate (R5P) for incorporation into nucleotides for DNA replication and RNA transcription. Among the enriched metabolic pathways, GSEA shows statistically significant enrichments of PPP, pyrimidine metabolism, and purine metabolism (KEGG: MMU00030, MMU00240, MMU00230) (Table 1, Figure 4C) in stimulated B cells. Consistent with these enriched gene set pathways, total and m+5 labeled R5P is massively increased (Figure 4D), providing a precursor for purine and pyrimidine biosynthesis. This m+5 label also tracks to downstream ribonucleotides, with less incorporation into deoxyribonucleotides (Figure S3C), despite markedly increased expression of *Rrm1/2* genes, which convert ribonucleotides to deoxyribonucleotides (Figure S3D). It is likely that at 24 hr, increases in transcription favor *de novo* biosynthesis of ribonucleotides over deoxyribonucleotides because DNA replication does not occur until after 24 hr of activation of B cells (Figure S3E).

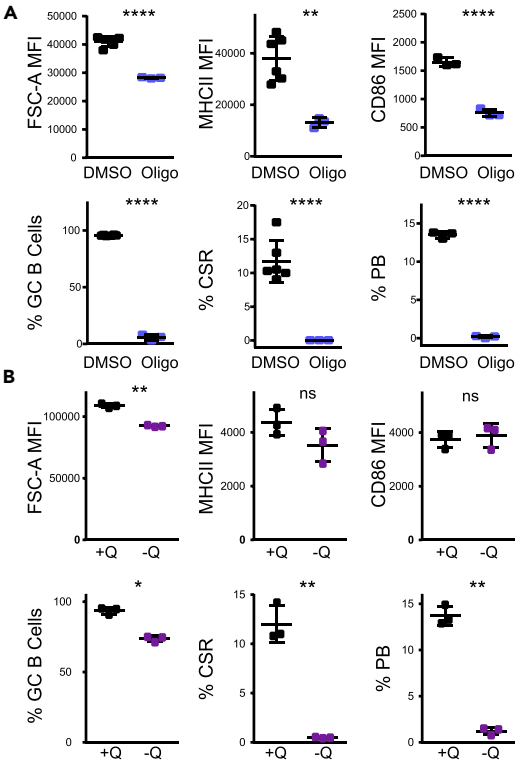

Figure 3. Perturbation of OXPHOS Negatively Affects B Cell Differentiation

(A) Flow cytometry analysis of cell size (FSC-A), activation markers (MHCII, CD86) at 24 hr, germinal center differentiation (GC, %B220+ Fas+ GL7+) and class switch recombination (CSR, %B220+ IgG1+) at day 3, and plasmablast differentiation (PB, %B220^{lo} CD138+) at day 5 in cells stimulated with DMSO or 10 nM Oligomycin A (n = 6 DMSO, n = 3 Oligo).

(B) Flow cytometry analysis of cell size (FSC-A), activation markers (MHCII, CD86) at 24 hr, germinal center differentiation (GC, %B220+ Fas+ GL7+) and class switch recombination (CSR, %B220 + IgG1+) at day 3, and plasmablast differentiation (PB, %B220^{lo} CD138+) at day 5 in cells stimulated with or without glutamine (n = 3).

Data represent mean ± SD. p Values determined by paired two-tailed Student's t test. *p ≤ 0.05; **p ≤ 0.01; ****p ≤ 0.0001.

Glucose carbons can also route toward the synthesis of lipids. GSEA metabolic signatures enriched for both terpenoid backbone biosynthesis and biosynthesis of unsaturated fatty acids (KEGG: MMU00900, MMU01040, respectively) (Table 1, Figure 4E), including transcript elevations for *Hmgcr*, the rate-limiting enzyme in cholesterol biosynthesis, and *Elovl6*, an enzyme involved in fatty acid elongation (Figure S3F). This suggests increased utilization of an elevated glucose flux toward the generation of lipids for stimulated B cells, which is compatible with a rapid replication rate. Although many nonpolar lipids are incompatible with ultra-high-performance liquid chromatography-MS on polar columns, we were able to detect isotopomer incorporation of glucose into cytidine disphosphate ethanolamine (CDP-ethanoloamine), a precursor for phosphatidylethanolamine, suggesting that glucose is indeed fluxing toward lipid generation. Also, despite previous findings showing incorporation of radiolabeled glucose into the predominant lipid species of cellular membranes, phosphatidylcholine (PC), upon stimulation with LPS (Dufort et al., 2014), we did not observe incorporation of glucose into PC by CD40/IL-4 stimulation (Figure 4F), suggesting that T cell stimulation mechanisms may program differential metabolic programs to support different biological demands. Overall, these data suggest that increased glucose uptake contributes mainly to the synthesis of biomass, including ribonucleotides and lipids, as stimulated B cells grow in preparation for rapid cell division.

Mitochondrial Remodeling in Response to B Cell Activation

Augmented TCA cycle and OXPHOS activation in stimulated B cells suggests the possibility for coordinate changes in mitochondrial dynamics and morphology. To evaluate mitochondria in living mouse B cells, we employed super-resolution Airyscan microscopy with tetramethylrhodamine, ethyl ester (TMRE), a mitochondrial membrane-potential dependent dye, and PicoGreen, a double-stranded DNA intercalation dye that marks both genomic and mtDNA. In naive B cells, we detected few, long mitochondria with multiple nucleoids per mitochondrion (Figures 5A and S4A). On average, each naive B cell had 2.6 mitochondria, which increased to an average of 5.0 mitochondria per B cell upon activation (Figure 5B). The average area of a single mitochondrion remained relatively stable, whereas the total mitochondrial area increased from 2.3 to 4.2 μm^2 (Figure 5B). The aspect ratio (long $axis_{object}$/short $axis_{object}$) of mitochondria showed higher ratios in naive cells, supporting our observations that naive B cells have longer mitochondria than stimulated B cells (Figure S4B). Circularity ($4\pi A$/perimeter^2) assessments also

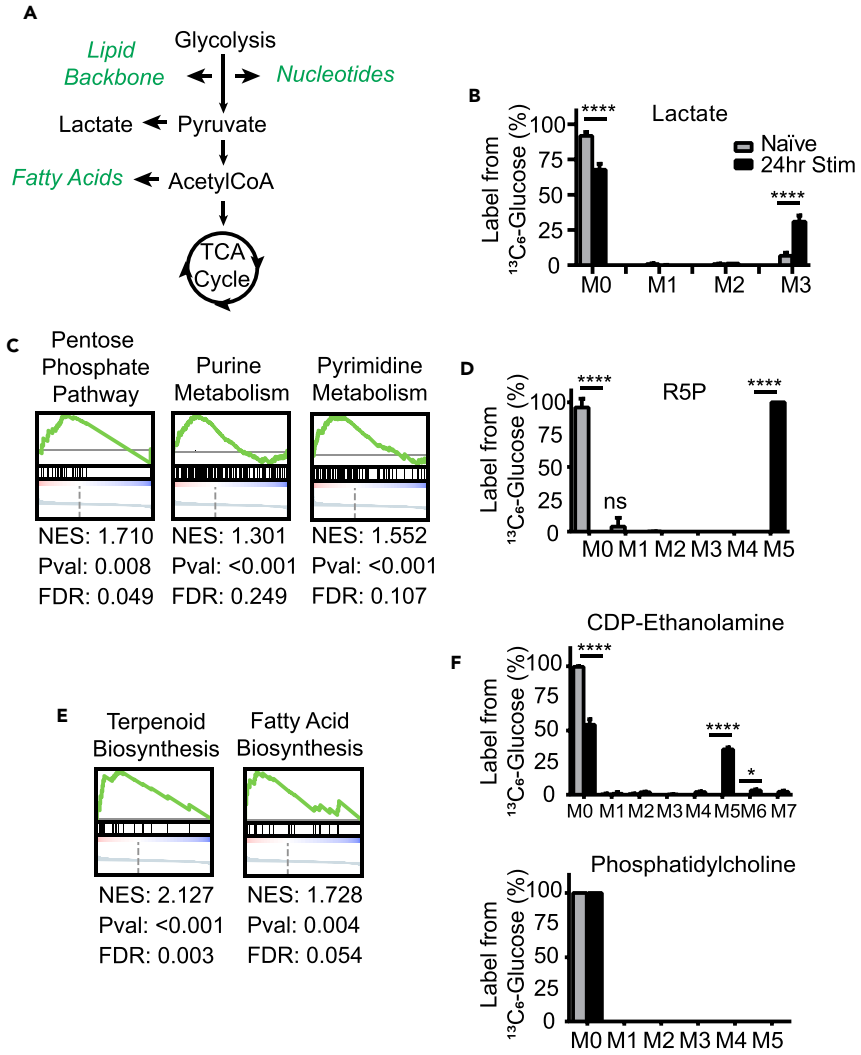

Figure 4. Additional Metabolic Pathways Utilize Carbon with B Cell Activation

(A) Schematic of potential main branch points for glucose-derived carbon utilization.

(B) Isotopomer distribution in naive and stimulated B cells for lactate (n = 3).

(C) GSEA on RNA-seq transcriptome data from naive and 24 hr stimulated B cells shows enrichment for PPP, pyrimidine, and purine metabolism transcripts.

(D) Isotopomer distribution of labeled glucose in R5P in naive and stimulated B cells (n = 3).

(E) GSEA for terpenoid biosynthesis and biosynthesis of unsaturated fatty acids.

(F) Isotopomer distribution of labeled glucose in CDP-ethanolamine and phosphatidylcholine in naive and stimulated B cells (n = 3).

Data represent mean ± SD. p Values determined by two-way ANOVA with Bonferroni correction for multiple comparisons. *p ≤ 0.05; ****p ≤ 0.0001.See also Figure S3, Tables S2 and S3.

reflect a greater roundness of mitochondria in activated B cells (Figure S4B). In agreement with OCR increases in activated B cells, we also detected an increase in mean TMRE fluorescence intensity at 24 hr (Figure S4B), reflecting an increase in proton gradients within the mitochondria.

A striking feature of activated B cells is the lack of an increase in mtDNA measured by qPCR despite increased mitochondrial numbers after stimulation (Figure 5C). Analysis of RNA-seq data for enrichment of KEGG pathways for genomic DNA and mtDNA replication (KEGG: MMU03030, MMU03029) are consistent with this result, as there is no significant change in the expression of mtDNA replication genes upon activation (Figure 5D). The total nucleoid number also does not increase with B cell activation; however, there is a decrease in the number of nucleoids per mitochondrion (Figure 5E). This is consistent with

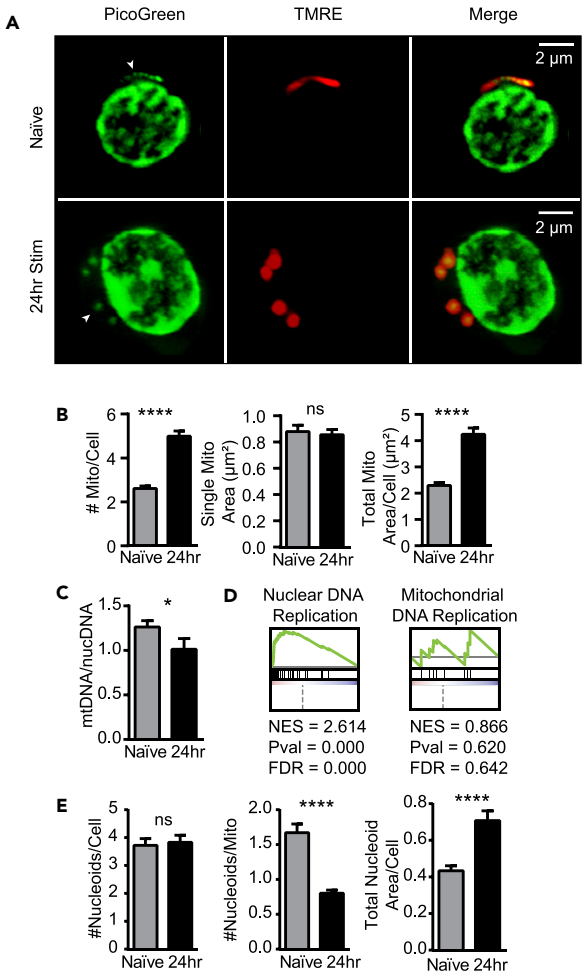

Figure 5. B Cell Activation Induces Mitochondrial Remodeling without Changes in mtDNA Levels

(A) Live-cell super-resolution imaging of primary naive and stimulated B cells stained with TMRE and PicoGreen (n = 120 naive cells, 90 stimulated from at least 3 biological replicates). Arrowheads indicate representative mitochondrial nucleoids. Scale bar represents 2 μm.

(B) Quantification of the number of mitochondria per cell, single mitochondrial area, and total mitochondrial area (n = 313 naive mitochondria from 120 cells, 447 stimulated mitochondria from 90 cells, all from at least 3 biological replicates).

(C) Ratio of mtDNA to genome DNA measured by qPCR (n = 3).

(D) GSEA for genome DNA and mtDNA replication shows no enrichment for mtDNA replication genes.

(E) Quantification of the number of nucleoids per cell, number of nucleoids per mitochondria, and total nucleoid area per cell (n = 120 naive cells, 90 stimulated from at least 3 biological replicates, n = 120).

Data represent mean ± SEM (B and D) or mean ± SD (C). p Values determined by unpaired two-tailed Student's t test. *p ≤ 0.05; ****p ≤ 0.0001. See also Figure S4.

our observation that naive B cells have fewer, elongated mitochondria with multiple nucleoids, and that stimulated B cells have more numerous and rounded mitochondria with a single nucleoid. Our data suggest that B cell mitochondria with multiple nucleoids undergo fission to generate more mitochondria without replicating their mtDNA, which agrees with minimal deoxyribonucleotide production at 24 hr activation (Figure S3B). Also, we detect little change in nuclear-encoded mitochondrial fission transcripts at 24 hr activation, although we do identify increases in the expression of MICOS complex genes, which are responsible for inner membrane remodeling (Cogliati et al., 2016) (Figure S4C). In addition, the total nucleoid area per cell increases with stimulation (Figure 5E), with increased nucleoid area previously suggested to represent increased mtDNA transcription (Alan et al., 2016; Lee and Han, 2017), consistent with increased emphasis on ribonucleotide production and augmented OXPHOS activity during the first 24 hr of B cell activation (Figure S3B). Combined, our data suggest a potential model in which B cells meet

increased demand for mitochondrial transcripts and OXPHOS during initial T cell-assisted activation by maintaining an expanded nucleoid pool in naive B cells, rather than by replicating mtDNA upon activation.

DISCUSSION

GC B cells are the fastest replicating non-cancerous cells in the human body, with little known about how they alter their metabolism from quiescence to support a massive numeric expansion to enable an effective humoral immune response. Using glucose isotopomer tracing we identified an unexpected decrease in total glycolytic metabolites with modeled T cell activation of naive B cells, with the exception of 3PG (Figure 1C). Increased 3PG may shunt toward synthesis of amino acids, and indeed, we detect increased total amounts of phosphoserine, serine, glycine, and threonine at 24 hr of activation (Figure S3G). Accumulation of 3PG may also suggest a block in pyruvate kinase (*Pkm1*), which catalyzes the conversion of phosphoenol pyruvate to pyruvate, or a switch to expression of the pyruvate kinase 2 (*Pkm2*) isoform. This switch has previously been observed in homocysteine-stimulated B cells (Deng et al., 2017) and occurs commonly in proliferating cells with a high level of nucleotide biosynthesis (Dayton et al., 2016).

A key unexpected finding was that glucose restriction had a relatively minor impact on T cell-dependent B cell activation (Figure 1D). Multiple studies have shown that B cells increase glucose uptake upon activation with multiple stimuli (Caro-Maldonado et al., 2014; Doughty et al., 2006; Garcia-Manteiga et al., 2011; Jellusova et al., 2017), yet B cells grown in only residual, 10-fold reduced glucose are able to activate and differentiate. The primary defects in glucose-restricted conditions were a minor decrease in cell size, likely from reduced contributions of glucose to the biosynthesis of lipids (Figures 4E and 4F) (Dufort et al., 2014), a minor increase in activation marker CD86, and a major defect in CSR of IgM to IgG1 (Figure 1E). It is unclear how glucose limitation may lead to reduced CSR; however, many of the signaling pathways required for B cell activation overlap with regulators of metabolic functions, including *Pax5*, *Myc*, and *Hif* (Boothby and Rickert, 2017). Further study is needed to tease apart the specific signaling pathways that link glucose metabolism to CSR.

Our surprising finding that glucose was largely dispensable for initial B cell activation prompted a more detailed study of metabolic pathways that support the energetic and biosynthetic requirements of B cell activation (Table 1). Analysis of an available RNA-seq dataset (Wöhner et al., 2016) enabled investigations of metabolic pathways utilized by CD40/IL-4-activated B cells. A caveat of this approach is that many metabolic processes are regulated allosterically rather than transcriptionally, including glycolysis, so we supplemented our studies with high-throughput metabolic tracing to evaluate consistency in our results. Specifically, we found that activated B cells upregulate OXPHOS and the TCA cycle (Figure 2A). Scant glucose is utilized in the TCA cycle (Figure 2D), suggesting that alternative carbon sources, such as glutamine, are anapleurotic fuels. Indeed, we and others have shown that B cell biomass accumulation, protein synthesis, and DNA replication, but not early activation, depend on glutamine (Figure 3B) (Heyse et al., 2015). Inhibition of OXPHOS with Oligomycin A substantially impaired B cell activation (Figure 3A). We cannot rule out, however, that Oligomycin A treatment may cause accumulation of reactive oxygen species (ROS), or that loss of mitochondrial function may cause other cellular phenotypes, such as lysosomal defects (Demers-Lamarche et al., 2016), that prevent usual B cell differentiation. Glutamine deprivation, however, phenocopies inhibition of OXPHOS by Oligomycin A (Figure 3A), which is at least consistent with glutamine utilization by the TCA cycle for supporting B cell functions. We also identified a flux increase in the PPP at 24 hr (Figure 4C), which, in addition to generating mainly ribonucleotides, provides reducing equivalents NADH and NADPH during this process. Activation of B cells induces intracellular ROS within the first 24 hr (Wheeler and Defranco, 2012), so PPP induction may also help maintain the B cell redox state.

Isotopomer tracing revealed 97% labeling of pyruvate in both naive and stimulated B cells; however, labeled pyruvate was not fully incorporated into lactate (Figure 4B) despite increases in *Ldha* expression. Previous studies have observed increased extracellular acidification rate (ECAR) upon B cell activation and have attributed this to increased lactate production (Caro-Maldonado et al., 2014; Jellusova et al., 2017); however, studies that specifically measure extracellular lactate (Garcia-Manteiga et al., 2011; Jellusova et al., 2017) did not find increases in actual lactate levels (Table S1). We propose that an ECAR increase originates from increased CO_2 and carbonic acid production from a highly active TCA cycle, and that activated B cells utilize pyruvate primarily for biosynthesis.

Pyruvate was not incorporated into lactate, but incorporation of labeled glucose carbons into the TCA cycle also did not appreciably occur (Figures 2D and 4B), leaving open the question of where pyruvate is

utilized. We hypothesize that pyruvate converts into acetyl-CoA and then incorporates into fatty acids, which is at least consistent with significant gene induction in this KEGG pathway (Table 1). In addition Dufort et al. (2014) have shown that LPS stimulation and IgM with IL-4 induce incorporation of radiolabeled glucose into polar and nonpolar lipids, although the ratios of the labeled lipids differ according to the stimulation condition, likely due to different bioenergetic needs for the final fates of each condition. Further studies of targeted metabolites will be required to determine the final fate(s) of pyruvate during the various stimuli of naive B cell activation.

Studies of mitochondria in primary lymphocytes have been limited, with prior work using transgenic T cells expressing fluorescent-tagged mitochondria (Ron-Harel et al., 2016) or low-resolution immunofluorescence imaging that lacked structural insights (Table S1) (Jellusova et al., 2017). Here, we imaged live B cells on a wild-type background by utilizing cell-permeable stains to study mitochondrial dynamics upon activation. This initial imaging study of mature B cell mitochondria provides some unexpected results. Similar to T cells, B cell activation causes changes in mitochondrial architecture. In direct contrast to T cells, however, there are ~50% fewer initial mitochondria in naive B cells (2.6/cell) than in naive T cells (~5.0/cell) (Ron-Harel et al., 2016) (Figures 5A and 5B). In addition, in T cells, increases in mitochondrial number accompany increases in mtDNA copy number, which does not occur in B cells. Instead, mtDNA and nucleoid numbers remain similar between naive and 24 hr stimulated B cells (Figure 5C). This may be due to naive B cells maintaining a larger mtDNA pool than thymocytes (Milasta et al., 2016). Further work is required to determine the benefits of this strategy for robust proliferation, activation, and differentiation, which aligns well with the delayed timing of genomic DNA replication and the initial preference for ribonucleotide synthesis during early B cell activation (Figures S3B and S3C).

The increased mitochondrial fragmentation upon stimulation, concordant with increases in OXPHOS, has only been reported for lymphocytes thus far. Canonically, longer, fused mitochondria are associated with increased OXPHOS, and smaller, fragmented mitochondria have less OXPHOS capacity and are associated with nutrient deprivation or OXPHOS inhibition (Galloway et al., 2012). This is an apparently distinct morphological strategy employed by lymphocytes. Perhaps in this highly proliferative system, B cells sacrifice mitochondrial morphology associated with efficient OXPHOS in favor of morphology that may promote additional mitochondrial pathways, such as one-carbon metabolism or calcium signaling.

In summary, we present a detailed investigation of the metabolic adaptations utilized by modeling T cell-dependent early B cell activation. By combining RNA-seq data with metabolomics, we uncovered metabolic pathways, fluxes, and strategies that support rapid B cell proliferation and expansion to initiate a humoral immune response. These findings broaden and deepen our understanding of the usual metabolic pathways that support B cell activation and the transition from quiescence to proliferation and differentiation, which may enable targeting of metabolic regulatory nodes to block autoimmunity and B cell leukemia and lymphoma.

METHODS

All methods can be found in the accompanying Transparent Methods supplemental file.

SUPPLEMENTAL INFORMATION

Supplemental Information includes Transparent Methods, four figures, and three tables and can be found with this article online at https://doi.org/10.1016/j.isci.2018.07.005.

ACKNOWLEDGMENTS

Flow cytometry was performed at the UCLA Broad Stem Cell Research Center Flow Cytometry Core. Metabolomics was performed at the UCLA Metabolomics Center by Daniel Braas. Seahorse Extracellular Flux analysis was performed at the UCLA Mitochondria and Metabolism Core by Linsey Stiles. We thank Heather Christofk for kind use of the NOVA Bioanalyzer. We thank Dr. Tara TeSlaa and Alexander J. Sercel for technical assistance and helpful discussions. Supported by the University of California Office of the President, UCLA Graduate Division (L.R.W.), and NIH grants GM007185 (L.R.W.), CA90571, CA156674, GM073981, CA185189, GM114188 (M.A.T.), and the Air Force Office of Scientific Research FA9550-15-1-0406 (M.A.T.).

AUTHOR CONTRIBUTIONS

Conceptualization, L.R.W., F.M.A., and M.A.T.; Methodology, L.R.W., D.M.W., O.S., and F.M.A.; Formal Analysis, L.R.W. and F.M.A.; Investigation, L.R.W., F.M.A., and D.M.W; Data Curation, F.M.A. Writing – Original Draft, L.R.W; Writing – Review & Editing, L.R.W., F.M.A., and M.A.T.; Visualization, L.R.W., F.M.A., and D.M.W.; Supervision, M.A.T. and O.S.; Funding Acquisition, L.R.W. and M.A.T.

DECLARATION OF INTERESTS

The authors declare no competing interests.

Received: November 17, 2017
Revised: May 31, 2018
Accepted: July 5, 2018
Published: July 27, 2018

REFERENCES

Alan, L., Spacek, T., and Jezek, P. (2016). Delaunay algorithm and principal component analysis for 3D visualization of mitochondrial DNA nucleoids by Biplane FPALM/dSTORM. Eur. Biophys. J. *45*, 443–461.

Boothby, M., and Rickert, R.C. (2017). Metabolic regulation of the immune humoral response. Immunity *46*, 743–755.

Caro-Maldonado, A., Wang, R., Nichols, A.G., Kuraoka, M., Milasta, S., Sun, L.D., Gavin, A.L., Abel, E.D., Kelsoe, G., Green, D.R., and Rathmell, J.C. (2014). Metabolic reprogramming is required for antibody production that is suppressed in anergic but exaggerated in chronically BAFF-exposed B cells. J. Immunol. *192*, 3626–3636.

Cho, S.H., Ahn, A.K., Bhargava, P., Lee, C.-H., Eischen, C.M., McGuinness, O., and Boothby, M. (2011). Glycolytic rate and lymphomagenesis depend on PARP14, an ADP ribosyltransferase of the B aggressive lymphoma (BAL) family. Proc. Natl. Acad. Sci. USA *108*, 15972–15977.

Cogliati, S., Enriquez, J.A., and Scorrano, L. (2016). Mitochondrial cristae: where beauty meets functionality. Trends Biochem. Sci. *41*, 261–273.

Dayton, T.L., Jacks, T., and Vander Heiden, M.G. (2016). PKM2, cancer metabolism, and the road ahead. EMBO Rep. *17*, 1721–1730.

Demers-Lamarche, J., Guillebaud, G., Tlili, M., Todkar, K., Belanger, N., Grondin, M., Nguyen, A.P., Michel, J., and Germain, M. (2016). Loss of mitochondrial function impairs lysosomes. J. Biol. Chem. *291*, 10263–10276.

Deng, J., Lu, S., Liu, H., Liu, B., Jiang, C., Xu, Q., Feng, J., and Wang, X. (2017). Homocysteine activates B cells via regulating PKM2-dependent metabolic reprogramming. J. Immunol. *198*, 170–183.

Doughty, C.A., Bleiman, B.F., Wagner, D.J., Dufort, F.J., Mataraza, J.M., Roberts, M.F., and Chiles, T.C. (2006). Antigen receptor-mediated changes in glucose metabolism in B lymphocytes: role of phosphatidylinositol 3-kinase signaling in the glycolytic control of growth. Blood *107*, 4458–4465.

Dufort, F.J., Bleiman, B.F., Gumina, M.R., Blair, D., Wagner, D.J., Roberts, M.F., Abu-Amer, Y., and Chiles, T.C. (2007). Cutting Edge: IL-4 mediated protection of primary B lymphocytes from apoptosis via Stat6-dependent regulation of glycolytic metabolism. J. Immunol. *179*, 4953–4957.

Dufort, F.J., Gumina, M.R., Ta, N.L., Tao, Y., Heyse, S.A., Scott, D.A., Richardson, A.D., Seyfried, T.N., and Chiles, T.C. (2014). Glucose-dependent de novo lipogenesis in B lymphocytes: a requirement for ATP-citrate lyase in lipopolysaccharide-induced differentiation. J. Biol. Chem. *289*, 7011–7024.

Galloway, C.A., Lee, H., and Yoon, Y. (2012). Mitochondrial morphology-emerging role in bioenergetics. Free Radic. Biol. Med. *53*, 2218–2228.

Garcia-Manteiga, J.M., Mari, S., Godejohann, M., Spraul, M., Napoli, C., Cenci, S., Musco, G., and Sitia, R. (2011). Metabolomics of B to plasma cell differentiation. J. Proteome Res. *10*, 4165–4176.

Heyse, S., Connolly, T., and Chiles, T. (2015). The regulation and role of L-glutamine in B-cell activation. FASEB J. *29*, 888.17.

Jellusova, J., Cato, M.H., Apgar, J.R., Ramezani-Rad, P., Leung, C.R., Chen, C., Richardson, A.D., Conner, E.M., Benschop, R.J., Woodgett, J.R., et al. (2017). Gsk3 is a metabolic checkpoint regulator in B cells. Nat. Immunol. *18*, 303–312.

Jellusova, J., and Rickert, R.C. (2017). A Brake for B Cell Proliferation: appropriate responses to metabolic stress are crucial to maintain B cell viability and prevent malignant outgrowth. Bioessays *39*, 1700079.

Lee, S.R., and Han, J. (2017). Mitochondrial nucleoid: shield and switch of the mitochondrial genome. Oxid. Med. Cell. Longev. *2017*, 8060949.

Milasta, S., Dillon, C.P., Sturm, O.E., Verbist, K.C., Brewer, T.L., Quarato, G., Brown, S.A., Frase, S., Janke, L.J., Perry, S.S., et al. (2016). Apoptosis-inducing-factor-dependent mitochondrial function is required for T cell but not B cell function. Immunity *44*, 88–102.

Ron-Harel, N., Santos, D., Ghergurovich, J.M., Sage, P.T., Reddy, A., Lovitch, S.B., Dephoure, N., Satterstrom, F.K., Sheffer, M., Spinelli, J.B., et al. (2016). Mitochondrial biogenesis and proteome remodeling promote one-carbon metabolism for T cell activation. Cell Metab. *24*, 104–117.

Rush, J.S., and Hodgkin, P.D. (2001). B cells activated via CD40 and IL-4 undergo a division burst but require continued stimulation to maintain division, survival and differentiation. Eur. J. Immunol. *31*, 1150–1159.

Stein, M., Dutting, S., Mougiakakos, D., Bosl, M., Fritsch, K., Reimer, D., Urbanczyk, S., Steinmetz, T., Schuh, W., Bozec, A., et al. (2017). A defined metabolic state in pre B cells governs B-cell development and is counterbalanced by swiprosin-2/EFhd1. Cell Death Differ. *24*, 1239–1252.

van der Windt, G.J., Everts, B., Chang, C.H., Curtis, J.D., Freitas, T.C., Amiel, E., Pearce, E.J., and Pearce, E.L. (2012). Mitochondrial respiratory capacity is a critical regulator of CD8+ T cell memory development. Immunity *36*, 68–78.

Vander Heiden, M.G., Lunt, S.Y., Dayton, T.L., Fiske, B.P., Israelsen, W.J., Mattaini, K.R., Vokes, N.I., Stephanopoulos, G., Cantley, L.C., Metallo, C.M., et al. (2011). Metabolic pathway alterations that support cell proliferation. Cold Spring Harb. Symp. Quant. Biol. *76*, 325–334.

Wheeler, M.L., and Defranco, A.L. (2012). Prolonged production of reactive oxygen species in response to B cell receptor stimulation promotes B cell activation and proliferation. J. Immunol. *189*, 4405–4416.

Wöhner, M., Tagoh, H., Bilic, I., Jaritz, M., Poliakova, D.K., Fischer, M., and Busslinger, M. (2016). Molecular functions of the transcription factors E2A and E2-2 in controlling germinal center B cell and plasma cell development. J. Exp. Med. *213*, 1201–1221.

ISCI, Volume *5*

Supplemental Information

Initial B Cell Activation Induces Metabolic Reprogramming and Mitochondrial Remodeling

Lynnea R. Waters, Fasih M. Ahsan, Dane M. Wolf, Orian Shirihai, and Michael A. Teitell

Supplemental Figures

- Figure S1: B cell isolation and activation. Related to Figures 1-4.
- Figure S2: Glucose-independent increase of the TCA cycle. Related to Figure 2.
- Figure S3: Alternative fates of glucose. Related to Figure 4.
- Figure S4: Mitochondrial remodeling with naïve B cell activation. Related to Figure 5.

Transparent Methods

Supplemental References

Supplemental Figures

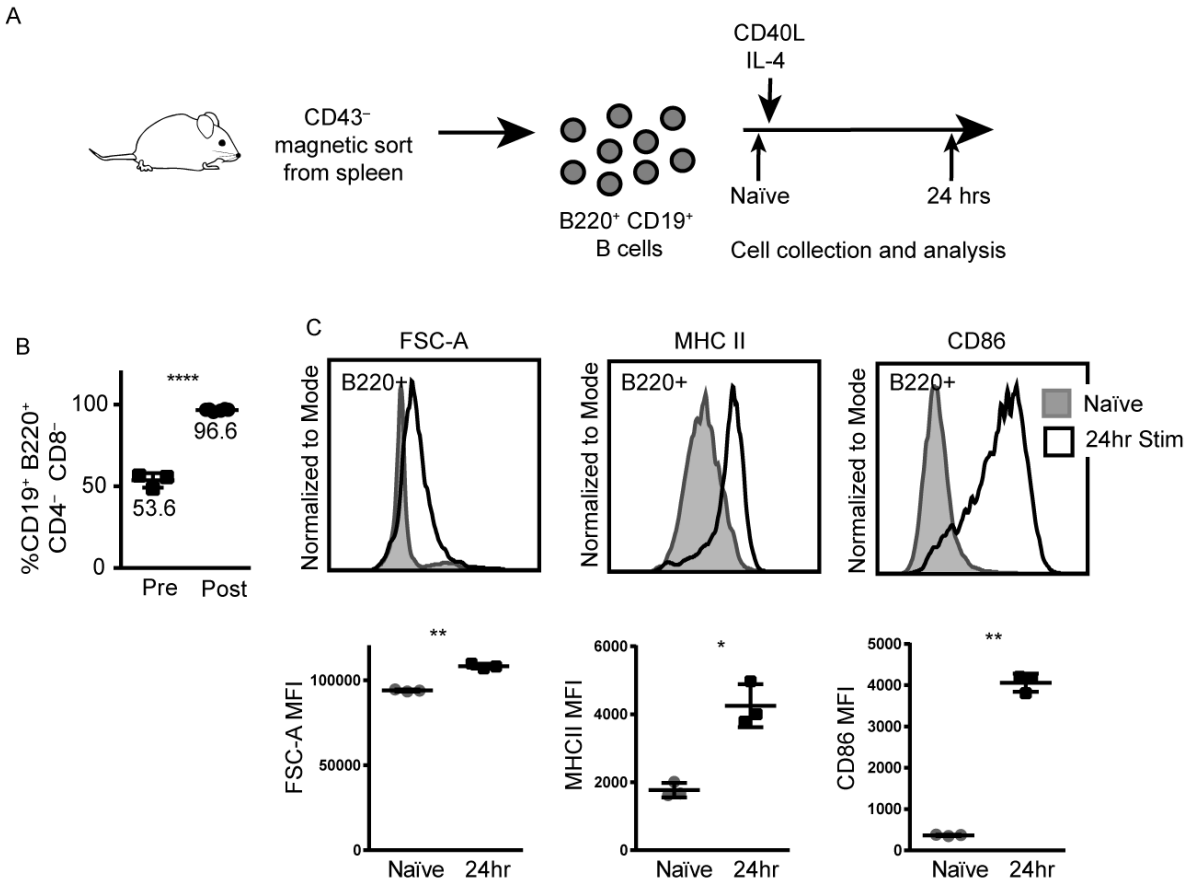

Figure S1: B cell isolation and activation. Related to Figures 1-4.

(A) Sorting scheme for isolating naïve mouse B cells. (B) Percentage of CD19+ B220+ CD4−CD8− B cells pre- and post-CD43 negative enrichment (*n*=3 pre, *n*=6 post). (C) Representative flow cytometry plots and analysis of cell size (FSC-A) and activation markers (MHCII, CD86) in naïve and 24 hr stimulated B cells (*n*=3). Data represent mean ± SD. p Values were determined by a paired two-tailed Student's *t*-test. *p ≤ 0.05, **p ≤ 0.01, ****p ≤ 0.0001.

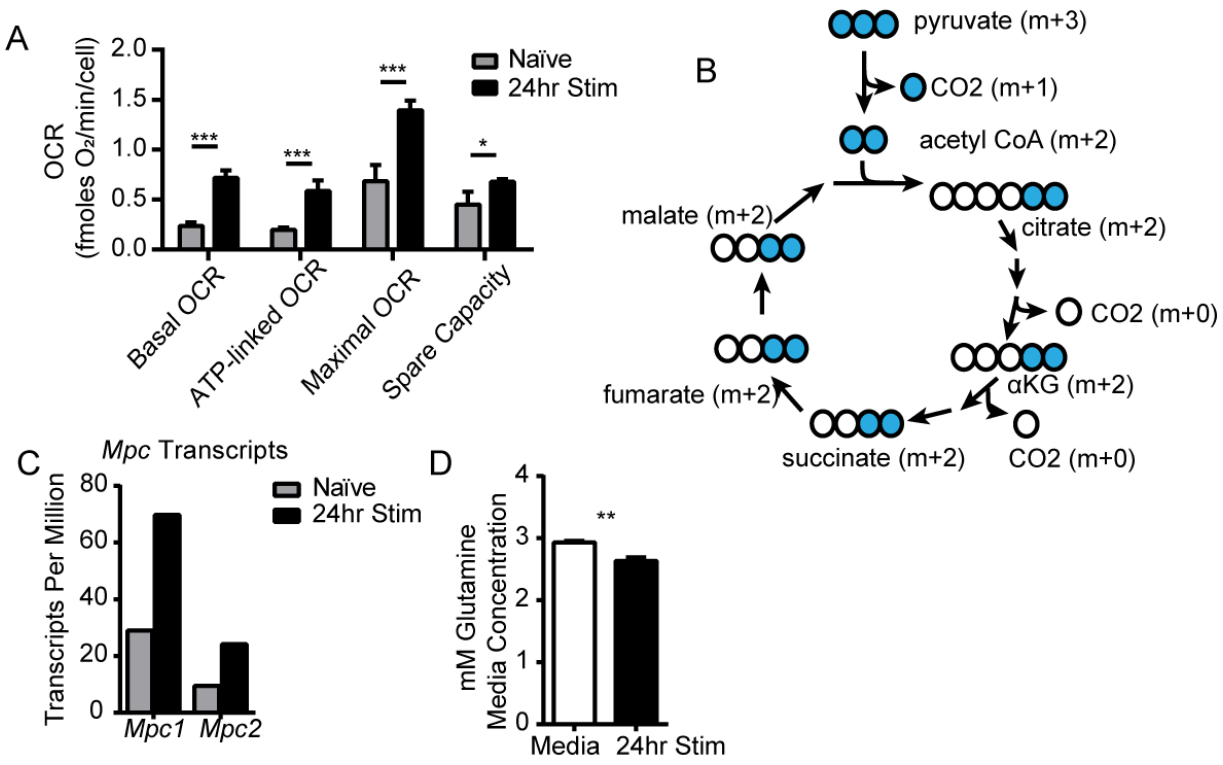

Figure S2: Glucose-independent increase of the TCA cycle. Related to Figure 2.

(A) Quantification of basal OCR, ATP-linked OCR, maximal OCR, and spare respiratory capacity (*n*=4). (B) Schematic of $^{13}C_6$-glucose isotopomer labeling (blue) of the TCA cycle. Incorporation of glucose results in increases in m+2 isotopomer accumulation. (C) Transcripts per million (TPM) for *Mpc1* and *Mpc2* expression in naïve and stimulated B cells extracted from RNA-Seq data (Wöhner et al., 2016). (D) Media glutamine concentration of full media and 24-hour stimulated cells (*n*=3 media, 5 stim). Data represent mean ± SD. p Values were determined by an unpaired two-tailed Student's *t*-test. *p ≤ 0.05, **p ≤ 0.01, ***p ≤ 0.001.

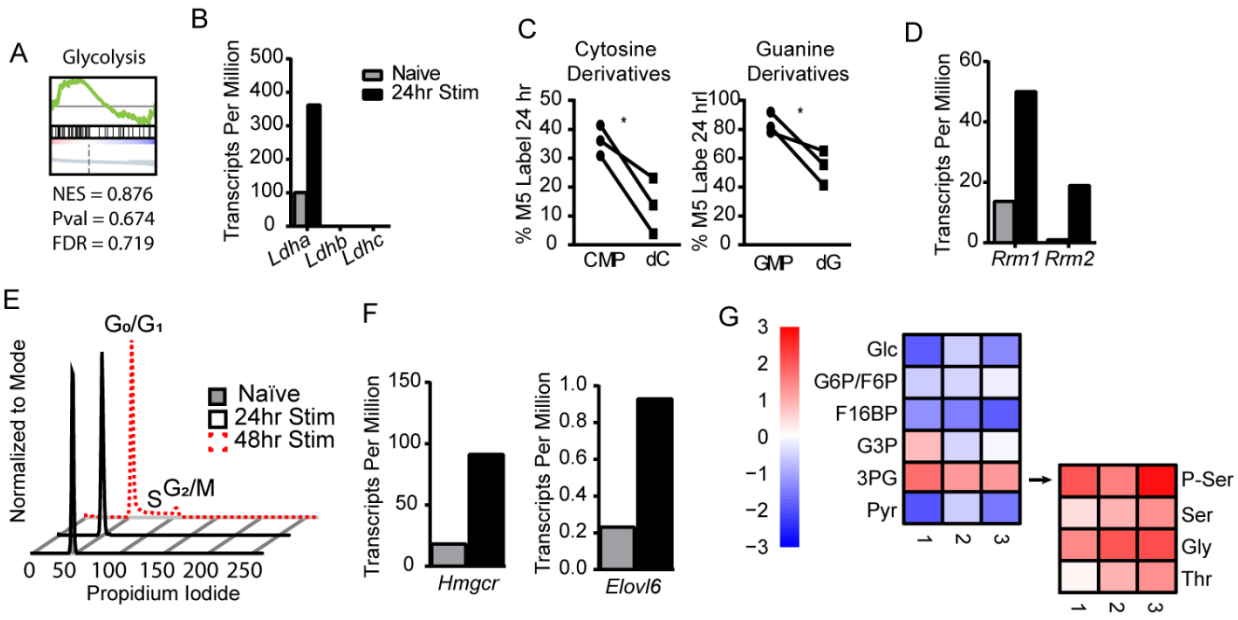

Figure S3: Alternative fates of glucose. Related to Figure 4.

(A) GSEA for glycolytic genes shows little enrichment in stimulated B cells. (B) Transcripts per million (TPM) for *Ldha*, *Ldhb* and *Ldhc* genes in naïve and stimulated B cells extracted from RNA-Seq data (Wöhner et al., 2016). (C) Percentage m+5 label at 24 hours of B cell activation in corresponding guanine and cytosine derivatives show decreased labeling of deoxyribonucleotides (*n*=3). (D) Transcripts per million (TPM) for *Rrm1* and *Rrm2* genes in naïve and stimulated B cells extracted from RNA-Seq data (Wöhner et al., 2016). (E) Cell cycle analysis of naïve and stimulated B cells shows no DNA replication until 48 hours after stimulation (*n*=3). (F) Transcripts per million (TPM) for *Hmgcr* and *Elovl6* genes in naïve and stimulated B cells extracted from RNA-Seq data (Wöhner et al., 2016). (G) UHPLC-MS quantification of relative levels of glycolytic metabolites and selected amino acids between stimulated and naïve B cells, data shown are $\log_2$ converted average values of 3 technical replicates of 3 biological replicates (*n*=3). p Values were determined by an unpaired two-tailed Student's *t*-test. *p ≤ 0.05.

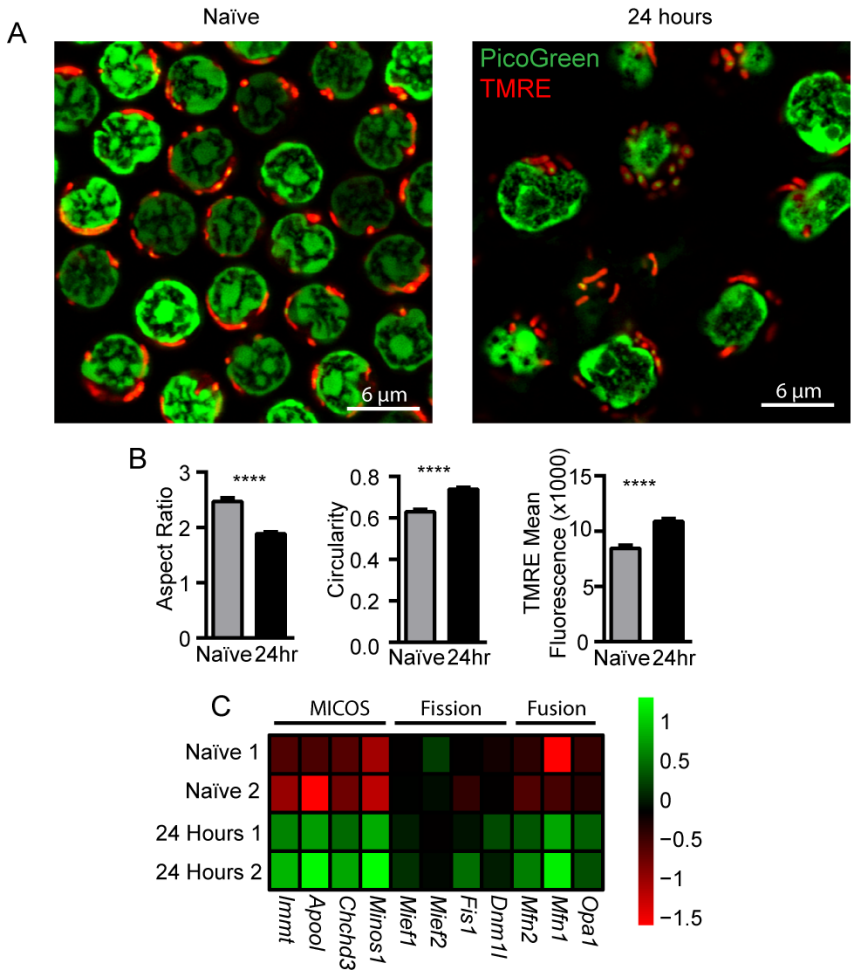

Figure S4: Mitochondrial remodeling with naïve B cell activation. Related to Figure 5.

(A) Representative field image from live cell super-resolution imaging of mouse naïve and 24 hour stimulated B cells stained with TMRE and PicoGreen (*n*=120 naïve cells, 90 stimulated from at least 3 biological replicates). Scale bar represents 6 µm. (B) Quantification of mitochondrial aspect ratio, circularity and TMRE mean fluorescence (*n*=313 naïve mitochondria from 120 cells, 447 stimulated mitochondria from 90 cells, from at least 3 biological replicates). (C) Heatmap of mitochondrial fission and fusion, and mitochondrial remodeling MICOS complex gene transcripts in naïve and 24 hour stimulated B cells. Values represent a variance-stabilized transformation of the count subtracted by the mean count of all samples. Data represent mean ± SD. p Values were determined by an unpaired two-tailed Student's t-test. ****p ≤ 0.0001.

Transparent Methods

Mice

C57BL/6J mice (Jackson Laboratory) were housed in a pathogen-free animal facility at UCLA. All mouse studies were on mixed-sex mice between 6 and 16 weeks of age with approval from the UCLA Institutional Animal Research Committee.

Stimulation of Primary Mouse B Cells

Red blood cell-lysed mouse spleen cells were enriched for B cells using CD43 negative magnetic selection (Miltenyi). Cells were grown in RPMI supplemented with 10% FBS and 50 μM β-mercaptoethanol. B cells were stimulated with 1 μg/ml αCD40 mAb (BD Pharmingen) and 25 ng/ml IL-4 (R&D Systems). At day 3, αCD40 was washed out and cells replated in media containing only IL-4 until day 5. For Oligomycin treatment, B cell media was supplemented with 10 nM Oligomycin A (Sigma) in DMSO.

Flow cytometry

Single cell suspensions were stained for 20 min in 50 μl FACS buffer (2% FBS in PBS) on ice in the dark. Data were obtained on a BD LSRII or BD Fortessa (BD Biosciences) and analyzed with FlowJo software (Treestar). Antibodies for flow cytometry included AlexaFluor700-B220, PE-CD4 (1:500), V450-CD86, V450-IgG1 (BD Horizon), APC/Cy7-CD19 (BioLegend), eFluor 450-CD8a, eFluor 450-GL7, AlexaFluor700-MHCII, AlexaFluor700-B220 (eBioscience), PE-CD95 (Fas), APC-CD138, PE-CD138 (BD Pharmingen) and PE-AlexaFluor610-B220 (Life Technologies) at 1:200 dilution unless indicated otherwise. Assessments of glucose import used a 2NBDG Glucose Uptake Assay Kit (Biovision) according to manufacturer instructions. For cell cycle analysis, cells were stained in hypotonic propidium iodide (PI) staining solution containing 10 mg/ml RNAse, 10% Triton X-100, 85 mg/ml trisodium citrate and 2 mg/ml PI (Roche).

Metabolomics

B cells were grown in glucose-free RPMI (Gibco) supplemented with 2 g/L [U-^{13}C] glucose (Cambridge Isotope Laboratories) and non-dialyzed FBS that contributed a residual 1.5 mM non-labeled glucose (data not shown). Metabolites were extracted with cold 80% methanol and measured using Ultra High Performance Liquid Chromatography Mass Spectrometry (UHPLC-MS), as previously described (TeSlaa et al., 2016; Thai et al., 2014). To extract intracellular metabolites, cells were pelleted by centrifugation (1000 RPM, 4°C) and rinsed with cold 150 mM ammonium acetate (pH 7.3), pelleted again, followed by addition of 1 ml cold 80% MeOH in water. To the cell suspensions, 10 nmol D/L-norvaline were added and rigorously mixed followed by centrifugation (1.3x10^4 rpm, 4°C). The supernatant was transferred into a glass vial and pellet was further extracted with 200 µl cold 80% MeOH in water. After centrifugation, supernatant was combined, metabolites dried down under vacuum, and resuspended in 70% acetonitrile. For the mass spectrometry-based analysis of the sample, 5 µl were injected onto a Luna NH2 (150 mm x 2 mm, Phenomenex) column. The samples were analyzed with an UltiMate 3000RSLC (Thermo Scientific) coupled to a Q Exactive mass spectrometer (Thermo Scientific). The Q Exactive was run with polarity switching (+3.50 kV / -3.50 kV) in full scan mode with an m/z range of 65-975. Separation was achieved using A) 5 mM NH4AcO (pH 9.9) and B) ACN. The gradient started with 15% A) going to 90% A) over 18 min, followed by an isocratic step for 9 min and reversal to the initial 15% A) for 7 min. Metabolites and isotopomers thereof were quantified with TraceFinder 3.3 using accurate mass measurements (≤ 3 ppm) and retention times. For isotopologue distribution measurements, data was corrected for naturally occurring 13C as described in (Moseley, 2010). Data analysis, including principal component analysis and hierarchical clustering was performed using the statistical language R. Fractional contributions were calculated using the formula $FC = \frac{\sum_0^n i*m_i}{n\sum_0^n m_i}$ as described in (Fendt et al., 2013), where m_i denotes the intensity of the isotopologue, and n marks the number of carbons

in a given metabolite. Data were normalized to cell counts. Relative amounts and isotopomer distribution values are included in a supplemental excel file (Table S2).

RNA-Seq Data Processing

Raw sequencing runs were downloaded for each wild-type primary naïve and stimulated B cell sample from NCBI SRA using SRA Toolkit (http://ncbi.github.io/sra-tools/), and filtered for low quality reads and adapter contamination using FastQC (http://www.bioinformatics.babraham.ac.uk/projects/fastqc), SeqTK (https://github.com/lh3/seqtk), and Cutadapt (Martin, 2011). Reads were quantified and quasi-mapped to the *Mus musculus* Gencode M15 (GRCm38.p5) reference transcriptome using the alignment-free transcript level quantifier Salmon v.0.8.2 (Harrow et al., 2012; Mudge and Harrow, 2015; Patro et al., 2017). The resulting estimated transcript counts were summarized into normalized gene level transcripts per million (TPM) and estimated count matrices using R (v. 3.4.0) Bioconductor (v. 3.5) package tximport (v. 1.4 - http://bioconductor.org/packages/tximport/).

The resulting sample gene count matrix was normalized and analyzed for differential gene expression using R (v. 3.4.0) Bioconductor (v. 3.5) package DESeq2 v1.16.0, estimating expression changes using an empirical Bayes procedure to generate moderated fold-change estimates (Huber et al., 2015; Love et al., 2014). Significance testing was performed using the Wald test, and resulting *P* values were adjusted for multiple testing using the Benjamini-Hochberg procedure (Benjamini and Hochberg, 1995). Differentially expressed genes (DEGs) were filtered using an adjusted false discovery rate (FDR) q value < 0.01.

Heatmaps were prepared using the variance-stabilized transformation of the count (VST). Values for each sample gene expression were calculated as the sample VST subtracted by the mean VST of all samples. Values were visualized using pheatmap (v. 1.0.8 - https://cran.r-project.org/web/packages/pheatmap/index.html/).

Gene set enrichment analysis (GSEA):

To determine scaled transcript per million (TPM) weighted pathway perturbations independent of significance testing cutoffs, we performed GSEA using the Broad Institute GSEA command line tool v2.2.4 (Mootha et al., 2003; Subramanian et al., 2005). Briefly, all genes with at least 1 TPM for any sample in the gene count matrix were input into the GSEA module and converted to their $\log_2$ ratio of class means. Normalized enrichment scores were calculated against 86 metabolic gene sets derived from the curated *Mus musculus* KEGG Metabolism Pathway Database (Kanehisa et al., 2012). Gene sets were filtered for a size between 15-500, scores were computed using the "classic" scoring scheme, and enriched gene sets were permuted 1,000 times and filtered with an FDR *q*-value < 0.25. GSEA calculations and plots were generated using Python 2.7.3 package GSEApy (https://pypi.python.org/pypi/gseapy).

List of GSEA results, gene sets tested, and transcript/gene-level expression values analyzed are included in a supplemental excel file (Table S3).

Accession

Samples and raw sequencing short read runs from analysis of GSE77744 (https://www.ncbi.nlm.nih.gov/geo/query/acc.cgi?acc=GSE77744) are under GEO Sample Accessions GSM2058395, GSM2058396, GSM2058399, and GSM2058400.

Seahorse XF Analysis

B cells were plated on PDL coated XF96-well plates at 750,000 cells/well for unstimulated, and 500,000 cells/well for 24 hour stimulated. Extracellular oxygen consumption rates were measured using a Seahorse XFe96 Extracellular Flux Analyzer (Agilent) in response to 1 µM oligomycin, first injection of 3 µM FCCP, second injection of 5.4 µM FCCP to ensure maximum respiration, and 1.5 µM rotenone/antimycin A. Data were normalized to cell counts.

NOVA

Glutamine levels in full media and after 24 hours were measured by plating 10^6 cells/ml in 2 ml, centrifuging to remove cells and debris, and analyzing using a BioProfile Basic Analyzer (NOVA Biomedical).

Live Cell Super-Resolution Imaging

Cells were plated in CELLview 4-well glass-bottom tissue culture dishes (Greiner Bio-One). 15 nM TMRE and 3 µl/ml PicoGreen (Molecular Probes) were added directly to cell culture media and incubated for 15 min (Ashley et al., 2005) before live-cell confocal imaging with an alpha Plan-Apochromat 100x/1.46 Oil DIC M27 objective on the Zeiss LSM 880 with Airyscan. Prior to analysis, raw images were automatically processed into deconvoluted Airyscan images using the Zen software. Image analysis was performed with FIJI (ImageJ) by subtracting background using a 50 pixel rolling ball radius and cropping 30 individual cells per experimental condition. Regions of interest were quantified by auto-thresholding the appropriate channel, despeckling the image by replacing pixels with the median value in its 3x3 neighborhood, and analyzing particles between 0.3-30 μm^2. ROIs were then measured and data transferred to Prism6 (GraphPad) for analysis.

mtDNA Quantification

Genome DNA and mtDNA content were quantified using real-time PCR with primers targeting *Cox1* and *Rps18* genes. DNA was isolated using the DNeasy Blood and Tissue Kit (Qiagen). qPCR was performed on a LightCycler480 (Roche) using SYBR Fast (Kappa Biostysems), 4 ng template DNA, and primers in a 10 µl reaction. Primer sequences were as follows:

Primer	**Sequence**
Cox1 F	5'-ACTTGCAACCCTACACGGAGGTAA-3'
Cox1 R	5'-TCGTGAACGACGATGTCAAGGGAT-3'
Rps18 F	5'-ACCTGTCTTGATAACTGCCCGTGT-3'
Rps18 R	5'-TAATGGCAGTGATGGCCAAGGCTA-3'

Statistical Analysis

Values are mean ± S.D. or S.E.M. Data were analyzed with Prism 6 (GraphPad). Parametric data were analyzed using paired or unpaired two-tailed Student's t-tests, or 2-way ANOVA with Bonferroni correction for multiple comparisons. For all data sets, $P<0.05$ was considered significant. *$P \leq 0.05$, **$P \leq 0.01$, ***$P \leq 0.001$, ****$P \leq 0.0001$.

Supplemental References

Benjamini, Y., and Hochberg, Y. (1995). Controlling the False Discovery Rate - a Practical and Powerful Approach to Multiple Testing. J Roy Stat Soc B Met *57*, 289-300.

Fendt, S.M., Bell, E.L., Keibler, M.A., Davidson, S.M., Wirth, G.J., Fiske, B., Mayers, J.R., Schwab, M., Bellinger, G., Csibi, A.*, et al.* (2013). Metformin decreases glucose oxidation and increases the dependency of prostate cancer cells on reductive glutamine metabolism. Cancer Res *73*, 4429-4438.

Harrow, J., Frankish, A., Gonzalez, J.M., Tapanari, E., Diekhans, M., Kokocinski, F., Aken, B.L., Barrell, D., Zadissa, A., Searle, S.*, et al.* (2012). GENCODE: the reference human genome annotation for The ENCODE Project. Genome Res *22*, 1760-1774.

Huber, W., Carey, V.J., Gentleman, R., Anders, S., Carlson, M., Carvalho, B.S., Bravo, H.C., Davis, S., Gatto, L., Girke, T.*, et al.* (2015). Orchestrating high-throughput genomic analysis with Bioconductor. Nat Methods *12*, 115-121.

Kanehisa, M., Goto, S., Sato, Y., Furumichi, M., and Tanabe, M. (2012). KEGG for integration and interpretation of large-scale molecular data sets. Nucleic Acids Res *40*, D109-114.
Love, M.I., Huber, W., and Anders, S. (2014). Moderated estimation of fold change and dispersion for RNA-seq data with DESeq2. Genome Biol *15*, 550.

Martin, M. (2011). Cutadapt removes adapter sequences from high-throughput sequencing reads. 2011 *17*.

Mootha, V.K., Lindgren, C.M., Eriksson, K.F., Subramanian, A., Sihag, S., Lehar, J., Puigserver, P., Carlsson, E., Ridderstrale, M., Laurila, E.*, et al.* (2003). PGC-1alpha-responsive genes involved in oxidative phosphorylation are coordinately downregulated in human diabetes. Nat Genet *34*, 267-273.

Moseley, H.N. (2010). Correcting for the effects of natural abundance in stable isotope resolved metabolomics experiments involving ultra-high resolution mass spectrometry. BMC Bioinformatics *11*, 139.

Mudge, J.M., and Harrow, J. (2015). Creating reference gene annotation for the mouse C57BL6/J genome assembly. Mamm Genome *26*, 366-378.

Patro, R., Duggal, G., Love, M.I., Irizarry, R.A., and Kingsford, C. (2017). Salmon provides fast and bias-aware quantification of transcript expression. Nat Methods *14*, 417-419.

Subramanian, A., Tamayo, P., Mootha, V.K., Mukherjee, S., Ebert, B.L., Gillette, M.A., Paulovich, A., Pomeroy, S.L., Golub, T.R., Lander, E.S.*, et al.* (2005). Gene set enrichment analysis: a knowledge-based approach for interpreting genome-wide expression profiles. Proc Natl Acad Sci U S A *102*, 15545-15550.

TeSlaa, T., Chaikovsky, A.C., Lipchina, I., Escobar, S.L., Hochedlinger, K., Huang, J., Graeber, T.G., Braas, D., and Teitell, M.A. (2016). alpha-Ketoglutarate Accelerates the Initial Differentiation of Primed Human Pluripotent Stem Cells. Cell Metab.

Thai, M., Graham, N.A., Braas, D., Nehil, M., Komisopoulou, E., Kurdistani, S.K., McCormick, F., Graeber, T.G., and Christofk, H.R. (2014). Adenovirus E4ORF1-induced MYC activation promotes host cell anabolic glucose metabolism and virus replication. Cell Metab *19*, 694-701.

Wöhner, M., Tagoh, H., Bilic, I., Jaritz, M., Poliakova, D.K., Fischer, M., and Busslinger, M. (2016). Molecular functions of the transcription factors E2A and E2-2 in controlling germinal center B cell and plasma cell development. J Exp Med *213*, 1201-1221.